C. R. Mecanique 340 (2012) 247–260

Contents lists available at SciVerse ScienceDirect

Comptes Rendus Mecanique

www.sciencedirect.com

Recent Advances in Micromechanics of Materials

# Interface controlled plastic flow modelled by strain gradient plasticity theory

Thomas Pardoen [a,*], Thierry J. Massart [b]

[a] Institute of Mechanics, Materials and Civil Engineering, Université catholique de Louvain, B-1348 Louvain-la-Neuve, Belgium
[b] Université Libre de Bruxelles (ULB), Building, Architecture & Town Planning Dept. (BATir), CP 194/02, Avenue F.D. Roosevelt 50, B-1050 Bruxelles, Belgium

ARTICLE INFO

*Article history:*
Available online 30 March 2012

*Keywords:*
Constitutive models
Strength
Ductility
Strain gradient plasticity
Size effects
Interfaces

ABSTRACT

The resistance to plastic flow in metals is often dominated by the presence of interfaces which interfere with dislocation nucleation and motion. Interfaces can be static such as grain and phase boundaries or dynamic such as new boundaries resulting from a phase transformation. The interface can be hard and fully impenetrable to dislocations, or soft and partly or fully transparent. The interactions between dislocations and interfaces constitute the main mechanism controlling the strength and strain hardening capacity of many metallic systems especially in very fine microstructures with a high density of interfaces. A phenomenological strain gradient plasticity theory is used to introduce, within a continuum framework, higher order boundary conditions which empirically represent the effect of interfaces on plastic flow. The strength of the interfaces can evolve during the loading in order to enrich the description of their response. The behaviour of single and dual phase steels, with possible TRIP effect, accounting for the interactions with static and dynamic boundaries, is addressed, with a specific focus on the size dependent strength and ductility balance. The size dependent response of weak precipitate free zones surrounding grain boundaries is treated as an example involving more than one microstructural length scale.



## 1. Introduction

The plasticity and fracture mechanisms of metallic polycrystals are often dominated by the presence of interfaces which constitute either barriers to dislocation motion, easy paths for deformation, nucleation sites for dislocations or twins and/or weak sites for the initiation of cracking. Interfaces can be much more dominant in setting the strength and ductility of metals than chemical composition and crystallography, especially in fine, ultra fine and nano-structured systems, e.g. [1–4]. The constraint exerted by the interfaces leads to local gradients of deformation which are physically accommodated by geometrically necessary dislocations (GNDs), e.g. [5–9]. The GNDs induce extra local hardening as well as back stresses. If the plastic gradients are large enough over regions that represent a significant portion of the volume of the deformed material, the overall response gets also modified, with distinct change of the hardening, isotropic strain hardening and kinematic hardening, hence of the strength and ductility. Furthermore, the effect becomes dependent on one or several characteristic dimensions of the microstructure typically set by the interface spacing and by the behaviour of the interfaces.

Strain gradient plasticity theories, e.g. [5,9–11] offer a theoretical framework to introduce, within a continuum description, the effect of interfaces on the plastic flow. The advantage of a continuum approach of plasticity is that it allows treating large, representative material systems, while injecting microstructural features, i.e. interfaces, through higher order

* Corresponding author.
*E-mail address:* thomas.pardoen@uclouvain.be (T. Pardoen).

1631-0721/$ – see front matter 
doi:10.1016/j.crme.2012.02.008

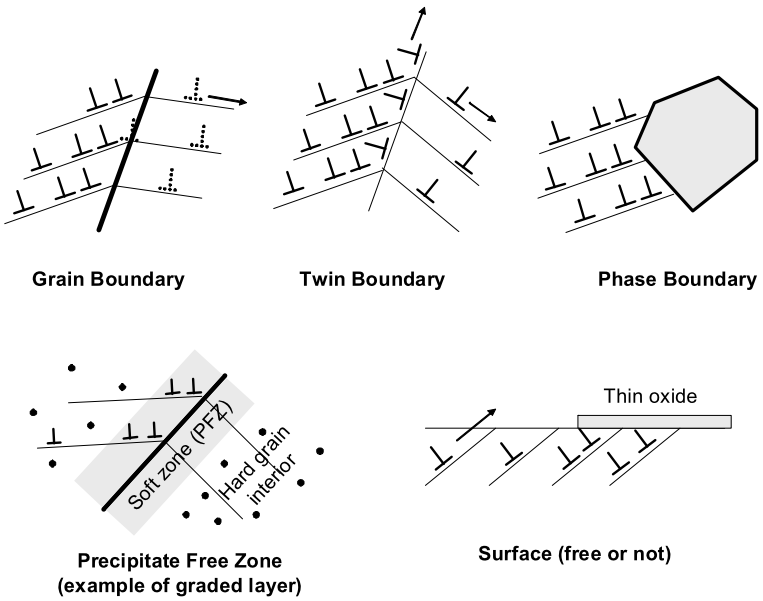


**Fig. 1.** Various kinds of interfaces in materials affecting dislocation activity by direct blocking, dislocation reactions, transmission above threshold stress, nucleation of new dislocations, annihilation, and generation of back stress.

boundary conditions. Treating the effect of interfaces through the use of higher order boundary conditions is not a trivial step and requires a good understanding of the physical interaction mechanisms in order to motivate the phenomenological choices. Many types of interfaces and of interactions are possible. Several of them are represented in Fig. 1:

- Grain boundaries (GB) constitute the ubiquitous example of boundaries. Physically, GB can produce different levels of constraint on dislocation motion, from fully impenetrable if the local stress is small enough to partly transparent if the stress is large enough to allow dislocations to fully or partly transmit. The dislocation/grain boundary interactions is a very complex problem, due the co-existence of multiple mechanisms such as blocking, annihilation, emission, reflection and transmission, depending on the stress level and character of the GB [2,12–14]. The convolution of these mechanisms has a direct impact on the rate of recovery near GBs and on setting the magnitude of the local strain gradients and of the resulting back stress. Reducing the grain size leads to an increase of the strength at the expense of the ductility. Now, GB can migrate under stress and constitute dynamic interfaces, e.g. [15,16].
- A twin boundary is a static boundary if it pre-exists before the loading such as in the case of annealed or growth twins. The interactions between the twin boundary and dislocation motion involve a combination of dislocation blocking with the creation of sessile and/or partial interface dislocations, and of transmission and generation of new dislocations; hence the nature (strength) of the interface evolves with deformation, see e.g. [4,17–20] for more details. Deformation twins constitute dynamic interfaces that multiply during deformation leading to an evolution of the microstructure characteristic lengths with even more profound impact on strain hardening than static twins, see e.g. [17,21–23].
- The effect of static phase boundaries regarding plastic flow is similar to GB if pre-existing in the material as a result of the processing routes, except that, most often, the in-coherency of the interface and the lattice mismatch between the phases make these interfaces impenetrable even at high stress levels. A proper selection of the volume fraction, size and morphology of the second phases is essential in the engineering of high performance metallic systems. An important class of dynamic phase boundaries involves stress and strain assisted phase transformation. TRIP steels [24–27] constitute a well known example where the controlled generation of a hard phase (with hard interfaces) in the microstructure during deformation provides a continuous source of strain hardening during deformation. Note that the specific case of precipitation hardening [28,29], in which the optimum precipitate size is on the order of a few nanometres, involves interactions with a small number of dislocations with a length scale that cannot realistically be treated by current continuum strain gradient plasticity theories.
- Graded materials involving steep evolutions of the microstructure over regions of the material can also be considered as an example of interfaces, though thicker and less sharp than the interfaces discussed above. A well known, usually unwanted example is provided by a variety of metallic alloys, such as Al, Ti, Ni or Fe based alloys, which involve micron or submicron thick layers surrounding GB with a microstructure different from the bulk of the grain, e.g. [30–32]. Often, these layers are softer than the rest of the grain, due to the absence of hardening precipitates which populate the grain interior (see Fig. 1), hence the name precipitate free zones (PFZ). The dislocations are not really blocked at the interface between the GB and PFZ but the plastic flow is constrained by the change of properties due to the change of local resistance to dislocation motion.

- Surfaces are interfaces which can be either completely transparent to dislocation if free [33] (and, in that case, the dislocations are attracted by the surface with a driving force pushing them to escape the crystal) or covered by a thin oxide layer or coating which can block the dislocations and raise the local strength, e.g. [34–36]. In the latter case, the interface response can evolve under the piling of dislocations which can lead to the cracking of the interface and the relaxation of the constraint.

Finally, the occurrence of plastic gradients can originate also from a non-uniform configuration of the loading, leading to size effects if the gradients are strong enough such as with nanoindentation, torsion of thin wires, submicron holes or bending of thin films [5,11,37,38]. This important category of problems was at the origin of the developments of the strain gradient plasticity theories. They are not addressed in the present paper.

The idea that strain gradient plasticity models can be used to introduce interface effects on plastic flow has been pursued by several authors. Gurtin, Gudmundson and their co-workers [7,10,39], followed by several others [9,40,41], enriched their higher order theories with a constitutive description of the interface response. More advanced models rely on crystal plasticity descriptions [42,43]. In the spirit of these studies, we have developed a generic approach of interfaces [36,44–47] in the context of a finite element model relying on a finite strain implementation of the strain gradient plasticity theory of Fleck and Hutchinson [48]. Cohesive zones are used to represent the interface layers, together with higher order boundary conditions. The novelty in the approach is to permit an evolution of the boundary conditions to mimic the effect of different phenomena such as new interfaces resulting from phase transformation, partial transparency of the GB at large stresses or an evolution of the coherency of a twin boundary. This model has been applied to a variety of size dependent strengthening effects dictated by interactions between interfaces and plastic flow.

The purpose of this article is to present the key ingredients of the strain gradient plasticity model with evolving interface conditions (Section 2) and to provide a few insightful illustrations. The first set of illustrations given in Section 3 summarises earlier findings about size dependent plasticity in single and dual phase steels with possible TRIP effect. In Section 4, an original set of results will be proposed regarding the problem of precipitate free zones in Al alloys which combine two types of interfaces and two length scales.

## 2. Model and numerical procedures

### 2.1. General model

A finite element model has been set up relying, for the material behaviour, on a finite strain implementation of the strain gradient plasticity theory by Fleck and Hutchinson [48]. The material is thus considered to deform through a "regular" plastic deformation mechanism by dislocation glide involving dislocation/dislocations interactions. Interface effects are considered here as in terms of the constraint on plastic flow induced by the dislocation/interface interactions. Crystal plasticity and interface fracture are not taken into account in this paper, though they can be incorporated within a similar framework. Traction separation laws are used to represent the interface layers, together with evolving higher order boundary conditions at the frontier with the material, see Fig. 2. An interface layer, whether it is a grain, a phase or a twin boundary, is usually extremely thin, on the order of one or a few atomic spacings, i.e. between 0.2 and 1 nm. The interface layer is considered as made of a truly different structure compared to the "bulk" material. When applying the load, the material starts deforming plastically first while the interface layer remains elastic.[1] The plastic flow at the frontier of the interface layer can be constrained by higher order boundary conditions from the most constrained by imposing zero plastic strain at the two sides of the interface, to the less constrained, by imposing no restriction on the plastic flow. Constraining the plastic flow leads to local plastic strain gradients, generating also a back stress, with a direct impact on the overall strength. Different conditions can be proposed to control the evolution of the boundary conditions. Here two models are used. In the case of GB, when the stress on the GB reaches a critical value, the constraint is relaxed on both sides of the GB and the plastic flow can develop at the interface. In the case of a phase boundary resulting from a phase transformation, a fully constrained interface is assumed at the boundary between the newly appearing and the parent phases when the transformation condition is met. In the simplest case considered here, the transformation criterion is based on a phenomenological transformation strain.

### 2.2. Material description

The material response is modelled using the strain gradient plasticity theory by Fleck and Hutchinson [48], extended to finite strains by Niordson et al. [49,50]. The gradient hardening effect enters through the generalised effective plastic strain $E_P$, defined as

$$\dot{E}_p^2 = \dot{\varepsilon}_p^2 + l_*^2 \dot{\varepsilon}_{p,i} \dot{\varepsilon}_{p,i} \tag{1}$$

[1] Physically, this is not always true. For instance, grain boundary sliding, which is a permanent deformation mechanism of an interface layer, could take place, in some circumstances, with the grain interior remaining elastic. These problems are not considered here.

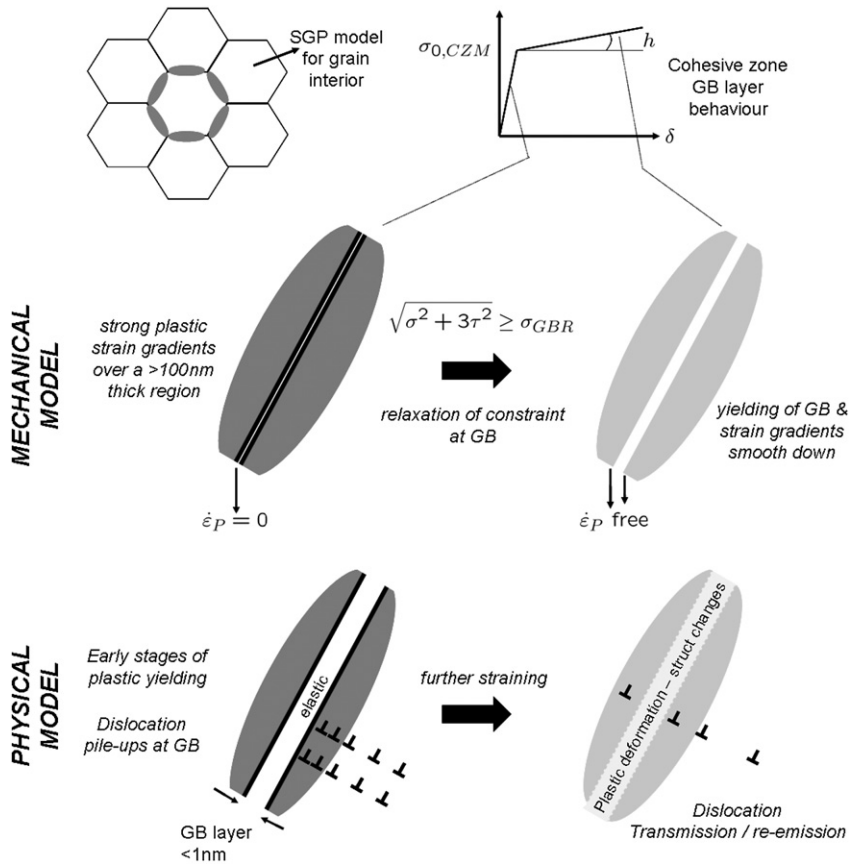


**Fig. 2.** Schematic description of the model for the polycrystal based on a strain gradient plasticity description of the grain interior and cohesive zone representation of the GB region involving, on both sides, interfaces with higher order boundary conditions. These interfaces are initially constrained (zero plastic flow) and the constraint can be relaxed when the stress on the GB attains a critical level.

where $\dot{\varepsilon}_p = \sqrt{\frac{2}{3}\dot{\varepsilon}^p_{ij}\dot{\varepsilon}^p_{ij}}$, $\dot{\varepsilon}^p_{ij}$ are the components of the plastic strain rate tensor, $\dot{\varepsilon}_{p,i}$ are the spatial gradients of the conventional equivalent plastic strain, and $l_*$ is a material length parameter. The general version of the theory with three internal lengths [48] is not addressed in this article.

The connection with the physics is that the length $l_*$ sets the scale of the gradient, whereupon the motions of the Geometrically Necessary Dislocations (GND) and Statistically Stored Dislocations (SSD) contribute equally to the hardening, see Evans and Hutchinson [51]. The plastic strain rate is given by the flow rule

$$\dot{\varepsilon}^p_{ij} = \dot{\varepsilon}_p \underbrace{\frac{3s_{ij}}{2\sigma_{(e)}}}_{m_{ij}} \tag{2}$$

where $s_{ij}$ are the components of the deviatoric part of the Cauchy stress tensor $\sigma_{ij}$ and $\sigma_{(e)}$ is the von Mises stress. Using a plastic strain field independent of the displacement field, the principle of virtual work expressed in the current configuration is [50]

$$\int_V \left(\sigma_{ij}\delta\dot{\varepsilon}_{ij} + (Q - \sigma_{(e)})\delta\dot{\varepsilon}_p + \tau_i\delta\dot{\varepsilon}_{p,i}\right) \mathrm{d}V = \int_S (T_i\delta\dot{u}_i + t\delta\dot{\varepsilon}_p)\,\mathrm{d}S \tag{3}$$

where $\varepsilon_{ij}$ is the total strain, $Q$ is the stress measure work conjugate to the conventional effective plastic strain, $\tau_i$ is the higher order stress conjugate to the spatial gradient of the conventional effective plastic strain, $T_i$ is the conventional traction at the boundary of the solid, and $t$ is the higher order traction at the boundary of the plastically deforming region. Using the determinant $J$ of the deformation gradient tensor, Kirchhoff stress measures are defined from the true stress measures as

$$\zeta_{ij} = J\sigma_{ij}, \qquad \sigma^{\zeta}_{(e)} = J\sigma_{(e)}, \qquad \rho_i = J\tau_i, \qquad q = JQ \tag{4}$$

Based on Eq. (3) and using an updated Lagrangian description ($J = 1$), the incremental form of the principle of virtual work can be expressed as follows [52]

$$\int_V \left(\overset{\nabla}{\zeta}_{ij}\delta\dot{\varepsilon}_{ij} - \sigma_{ij}(2\dot{\varepsilon}_{ik}\delta\dot{\varepsilon}_{kj} - \dot{e}_{kj}\delta\dot{e}_{ki}) + \left(\dot{q} - \dot{\sigma}^{\zeta}_{(e)}\right)\delta\dot{\varepsilon}_p + \overset{\vee}{\rho}_i\delta\dot{\varepsilon}_{p0,i}\right) \mathrm{d}V = \int_S (\dot{T}_{0i}\delta\dot{u}_i + \dot{t}_0\delta\dot{\varepsilon}_p)\,\mathrm{d}S \tag{5}$$

where $\dot{\varepsilon}_{p0,i}$ denotes derivatives with respect to the initial coordinate system, the '0' index denotes a nominal quantity, $\dot{e}_{ij}$ is the gradient of the displacement rate, and the symbols $^{\nabla}$ and $^{\vee}$ denote, respectively, Jaumann and convected rates. The finite strain generalisation of the constitutive equations reads

$$\overset{\nabla}{\zeta}_{ij} = L_{ijkl}(\dot{\varepsilon}_{kl} - \dot{\varepsilon}_p m_{kl}), \qquad \dot{q} = h(E_p)\dot{\varepsilon}_p, \qquad \overset{\vee}{\rho}_i = l_*^2 h(E_p)\dot{\varepsilon}_{p,i} \tag{6}$$

The hardening modulus $h(E_P)$ is evaluated based on the 'conventional' hardening rule selected for the behaviour of the "ideal" material with no interfaces, i.e. a single phase polycrystal with a very large grain size. Two types of hardening rules are used. For polycrystal simulations, a Voce-type law is used as

$$\sigma = \sigma_0 + \frac{\Theta_0}{\beta}\left(1 - \exp(-\beta E_P)\right) \tag{7}$$

For the analysis of the TRIP effect, a Swift-type hardening law is used which reads

$$\sigma = \sigma_0(1 + \varepsilon_0 E_P)^N \tag{8}$$

from which the hardening modulus can be obtained by derivation. Note that the use of an additional plastic strain field requires the imposition of specific boundary conditions at the boundary of the (evolving) plastic zone. In the present contribution, no higher order confinement is considered at the moving elastoplastic boundaries. The boundary conditions at the physical interfaces are discussed next.

### 2.3. Model for the interface layer

The interface region behaviour is empirically lumped into a cohesive zone (CZ) description. There are two key aspects associated to the explicit introduction of interfaces: the introduction of higher order boundary conditions applied on both faces of these interface elements and the traction separation response of the interface layer. As sketched in Fig. 2, the behaviour of an interface layer is first elastic with the following relationship

$$\begin{bmatrix} \tau \\ \sigma \end{bmatrix} = \begin{bmatrix} E/w & 0 \\ 0 & G/w \end{bmatrix} \begin{bmatrix} \Delta u_t \\ \Delta u_n \end{bmatrix} \tag{9}$$

where $w$ is the initial thickness of the interface layer (on the order of 1 nm), $E$ and $G$ are the Young's and shear modulus, respectively, and $\Delta u_t$ and $\Delta u_n$ represent the tangential and the normal displacement, respectively. The elastic parameters of the CZ are considered equal to the mean value of the elastic parameters of the two surrounding grains.

The plastic flow is initially constrained by using the cohesive zone to impose the condition $\dot{\varepsilon}_p = 0$ through a penalty term at the boundary of the grain interior. Upon further straining, the confinement condition can be modified [44–47] based on a condition on the local (conventional) stress carried by the CZ. The condition for relaxing the higher order confining effect is formulated in terms of the CZ von Mises stress as

$$\sigma_{eq} = \sqrt{\sigma^2 + 3\tau^2} \geqslant \sigma_{IR} \tag{10}$$

where $\sigma_{IR}$ is the phenomenological parameter governing the relaxation of the constraint, named interface relaxation stress.

The elastic response is followed by a linear hardening response of the interface (see Fig. 2)

$$\sigma_{y,CZ}(\kappa) = \sigma_{0,CZM} + h_I\kappa \tag{11}$$

where $\kappa$ is the hardening parameter taken as the equivalent plastic opening of the CZ and $\sigma_{0,CZM}$ is the initial yield stress of the CZ. The plastic behaviour of the CZ representing the interface behaviour is assumed to follow an associated flow rule. The fact that $\sigma_{IR}$ can be different than $\sigma_{0,CZM}$ offers additional degrees of freedom for the adjustment of the interface response. Now, physically, it is not easy to distinguish these two quantities. One could envision that for a mechanism of dislocation transmission controlled by a critical stress value, the two terms would be equal. If grain boundaries play the role of dislocation sources, the term $\sigma_{0,CZM}$ could be for instance smaller than $\sigma_{IR}$ meaning that plasticity can be activated in the interface, while the GB could still remain impenetrable to gliding dislocations. Also, this degree of freedom allows accounting (phenomenologically) for other mechanisms of deformation taking place at the interface such as GB sliding, independently of the constraint on the plastic flow in the surrounding material.

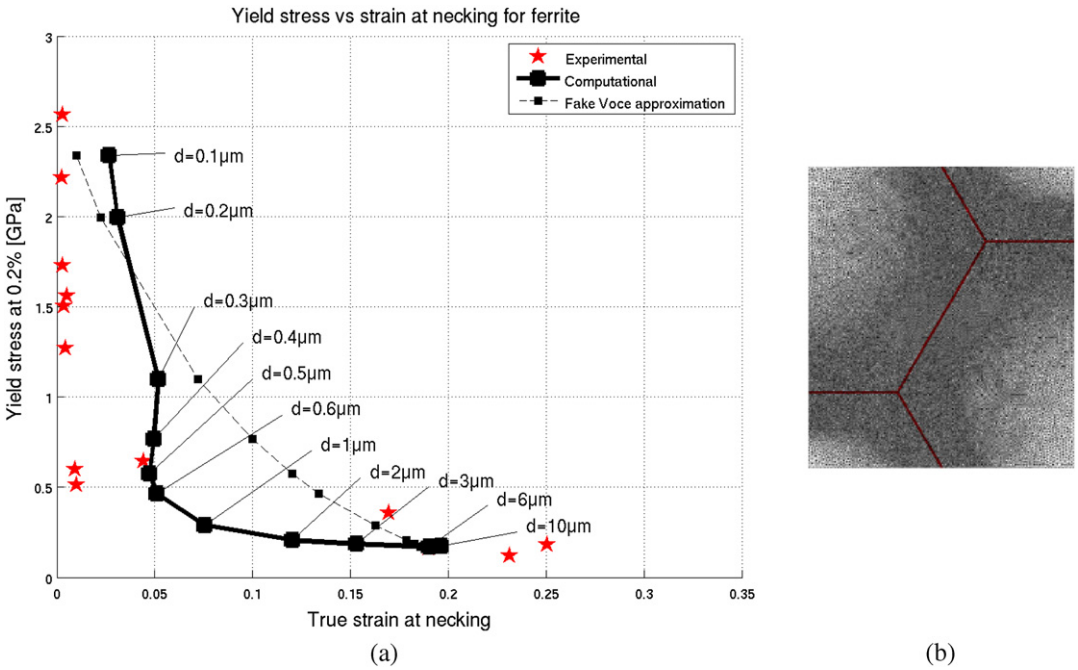


**Fig. 3.** Predicted yield stress versus uniform elongation in uniaxial tension corresponding to properties of ferritic steel with different grain sizes. Computational values are obtained using interface enriched strain gradient plasticity and the Considère criterion to determine the occurrence of necking. Experimental values are obtained from [59]. The dashed line represents the result obtained by a Voce law.

### *2.4. Numerical procedures*

The detailed finite element implementation of the strain gradient plasticity framework is described in Refs. [49,50]. The code is limited to 2D boundary value problem, under plane stress or plane strain conditions. The implementation is purely incremental, which means that the variations of the displacements and of the effective plastic strains are computed at each step. Essential boundary conditions may therefore be prescribed on these variations at each calculation step. Due to the purely incremental nature of the description, a refined time step is used. Triangular elements are used with a quadratic interpolation of the displacement field and linear interpolation of the plastic strain field. Care is taken to produce very refined mesh near the interface boundaries in each discretisation, with 15 to 20 elements over a distance corresponding to the dominant intrinsic length $l_*$, in order to properly capture the plastic strain gradients.

## 3. Size dependent strength and ductility in single and dual phase steels

The model described in Section 2 has been used to better understand the size dependent strength and ductility balance evolution observed when changing the interface density in a variety of steels from simple single phase ferritic steels to complex TRIP-aided multiphase steels. The gradation in complexity comes from that single phase steels involve only GB, while dual phase steels exhibit both GB and phase boundaries, and TRIP steels imply also an evolution of one of the phases which transforms during deformation. The message focuses on the importance of accounting for an enriched description of the interfaces to capture the strength ductility balance of these materials. Only uniaxial tension conditions are considered. The ductility is defined as the resistance to plastic localisation and predicted by the Considère condition.

### *3.1. Single phase ferritic steels*

The famous Hall–Petch effect [53] refers to the increase of the strength proportional to the inverse of the grain size to a power roughly equal to 1/2. The Hall–Petch effect can be predicted with a variety of models relying on different physical assumptions, e.g. [54]. Now, when decreasing the grain size, the ductility, quantified by the uniform elongation, also decreases. An example is given in Fig. 3 for ferritic steels. The experimental data, collected by Bouaziz [55] either for pure iron [56,57] or interstitial free (IF) steels [55,58,59] and covering grain sizes $d$ varying between 80 nm and 80 μm, involve variations of the yield stress and of the ductility both by more than a factor 20. This range of grain size is known to encompass different dislocations mediated mechanisms [60] from those met: (i) in Ultra Fine-Grained (UFG) materials with $d < 0.1$–$0.2$ μm with limited dislocation storage and all the dislocation activity at the GB; (ii) in the transitional behaviour of Fine-Grained (FG) materials; and (iii) in the traditional regime ($d > 1$–$2$ μm) involving abundant dislocation storage. This size dependent loss of ductility in fine- and ultra fine-grained metals is a major technological issue.

The FE model used to analyse the effect of the grain size in ferritic steels is a unit cell representing, with appropriate symmetries, the response of a polycrystal made of identical hexagonal grains, with all grains exhibiting the same properties. Only one half of the representative unit cells is modelled owing to the symmetries of the geometry. Periodicity is enforced by keeping the vertical boundaries straight and vertical during deformation and by imposing periodicity constraints on displacements and equivalent plastic strains between top and bottom boundaries. The flow properties of a pure ferrite have been determined based on an experimental flow curve corresponding to a large grain size $d = 10$ μm (assimilated as the infinite grain size limit $d \to \infty$), using the Voce law (7) giving $\sigma_0 = 150$ MPa, $\Theta_0 = 2.6$ GPa, and $\beta = 10$. The Young's modulus $E$ is set equal to 200 GPa and the Poisson ratio $\nu$ is equal to 0.3. The length $l_* = 0.8$ μm was adjusted to exactly predict the yield strength corresponding to an intermediate grain size $d = 500$ nm. The value $l_* = 0.8$ μm agrees with the typical lengths reported in the literature, e.g. [48,51]. Finally, the interface relaxation stress $\sigma_{IR}$ was tuned in order to capture the yield strength corresponding to $d = 100$ nm, giving $\sigma_{IR} = 15\sigma_0 = 2.25$ GPa. A very low strain hardening $h_I = 0.1$ MPa of the GB was assumed at this stage, and the initial width $w$ associated with the CZ was taken equal to 0.5 nm. FE simulations were then performed for grain sizes varying between 100 nm and 10 μm.

As shown in Fig. 3, the model captures the yield stress evolution, as well as the drop of ductility taking place at a grain size around 1 μm, and this, using a single, constant internal length. Relaxation of the GB constraint is needed to correctly predict the response at the smallest grain sizes. Indeed, accounting for the presence of impenetrable GB only with no relaxation of the constraint, i.e. $\sigma_{GBR} = \sigma_{0,CZM} = \infty$, reproduces the trend correctly except for the small grain sizes for which the yield strength is significantly overestimated as well as the ductility, see [46]. GB relaxation also leads to an additional decrease of the strain hardening capacity at the smallest grain sizes. At even smaller grain size, typically smaller than 20–40 nm, mechanisms such as grain boundary sliding, will obviously change this picture [2,3]. Fig. 3 also shows the results predicted directly with a "fake" Voce hardening law (thus without any FE calculations) with the yield stress corresponding to the measured yield stress for each grain size while keeping the parameters $\Theta_0$ and $\beta$ constant. Fig. 3 shows that the ductility does indeed decrease with the increase of strength as expected from the Considère criterion, but the variation is smooth and does not capture the sharp transition around $d = 1$ μm. Finally, the back stress was found to increase with decreasing grain size, see [46].

### 3.2. Dual phase steel

A dual phase steel is a composite material made of a ferritic matrix and a dispersion of hard martensitic islands [61]. This family of high strength steel is increasingly used, especially in the automotive industry where strength is not the only property of interest. Resistance to plastic localisation with respect to forming operations and a demand on crash-worthiness require a sufficiently large ductility. The question is to determine if the introduction of a second phase in a very fine-grained ferritic matrix could help recovering some of the lost ductility (see the previous section) while preserving the high strength. Delincé et al. [62] have predicted the existence of an optimum intermediate grain size depending on the volume fraction of second phases; the grain size effect was introduced within a simple physics based 1D framework. Here, the model presented in Section 2 is applied in order to simulate the complex plastic flow taking place in the DP steels. The starting point is a set of experimental data, involving three dual phase steels called: "CG" for "coarse grains", "FG" for "fine grains" and "VFG" for "very fine grains". The details of the processing and microstructure characterisation are given in Refs. [62, 63]. The microstructure of the CG, FG and VFG specimens consists of a ferritic matrix with dispersed martensite inclusions located along the ferrite GBs. The average grain size of the ferrite phase is equal to 6.6 μm, 1.7 μm and 1.1 μm for the CG, FG and VFG steels, respectively. The volume fraction of second phase is equal to 34%, 26% and 22% for the CG, FG and VFG steels. The martensite grain size varies moderately between the CG steels and the two finer grained steels. Fig. 4b shows the stress–strain curves; clearly, the FG steel leads to the best strength/ductility balance.

Representative volume elements of the CG, FG and VFG steels were extracted from high magnification micrographs, with a size of respectively $10\times10$ μm$^2$, $5\times5$ μm$^2$ and $5\times5$ μm$^2$, and containing respectively 15, 28 and 54 grains. This size was selected to provide a trade off between representativeness and computational time. These typical cells are shown in Fig. 4a.

The elastic properties were taken identical for the two phases with Young's modulus equal to 200 GPa and Poisson ratio equal to 0.3. The initial yield stress of the ferrite phase for an assumed infinite grain size (thus without any gradient effect) was taken equal to $\sigma_{0,f} = 250$ MPa [62]. This value for ferrite is increased with respect to the one used in Section 3.1 for pure ferrite and IF steels, owing to its carbon (C) content in DP steels and to the potential presence of carbides. The yield stress of the martensite phase is dependent on the C content, see e.g. [64]. The total C content is equal to 0.15%. By considering that the volume fraction of C in the ferrite amounts to 0.05% (i.e. 0.025% limit of solubility + an estimated 0.025% trapped in carbides), the C content in the martensite is equal to 0.5%, 0.43% and 0.34% in the CG, FG and VFG DP steels, respectively. Based on the results in Ref. [65], the corresponding yield stress is equal to $\sigma_{0,m} = 1100$, 1050 and 1000 MPa, for the CG, FG and VFG DP steels, respectively. The Voce law parameters of the martensite phase were selected as equal to $\Theta_{0,m} = 400$ GPa, $\beta = 615$ based on the data by Cobo and Bouaziz [65], neglecting the change of strain hardening capacity with changing C content. For the sake of simplicity, the same intrinsic length was chosen for both martensite and ferrite $l_m = l_f = l_*$. Each interface is characterised by a yield stress $\sigma_{0,CZM}$, a hardening coefficient $h_I$, and a relaxation stress $\sigma_{IR}$. The flow properties of the ferrite phase have been selected in the following way. The parameters of the Voce law $\beta_f$ and $\Theta_{0,f}$ were fitted on the CG curve with different intrinsic lengths $l_*$ [300, 400, 600, 800] nm. Simulations were then performed for the FG and VFG samples using the identified values for the different lengths $l_*$. The best match for all three

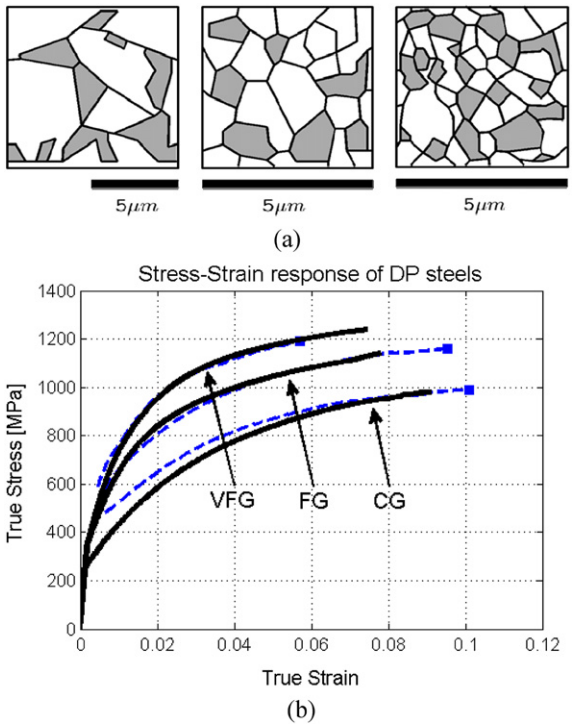


**Fig. 4.** Size effect in DP steels: (a) periodic unit cells used for the homogenisation computations for coarse-grained, fine-grained and ultra fine-grained samples (the dark phase depicts martensitic inclusions), (b) yield stress versus strain at necking for the three samples.

CG, FG, VFG curves on the first 2–3% of deformation was found for $l_f = l_m = 300$ nm. Finally, the relaxation stress on the ferrite GBs was adjusted to obtain a fit on the FG curve for the larger deformations leading to $\sigma_{0,CZMferr} = \sigma_{IRferr} = 650$ MPa. The Voce flow parameters are equal to $\beta_f = 10.5$ and $\Theta_{0,f} = 6.4$ GPa. All the interfaces connected to the martensite are impenetrable to dislocations up to a stress level $\sigma_{IR} = 2000$ MPa, and have the same yield stress. This value was adjusted in order to fit the VFG curve at large strains.

The comparison between the model and the experimental results is given in Fig. 4b. One cannot really consider this comparison as a validation as all the available data were used to identify the parameters of the model. Still, the model is rich enough to capture all the trends: it is possible to predict the complex interplay between the deformation mechanisms and the microstructure with the ingredients of the model described in Section 2. The model can then be used with the identified parameters to guide the optimisation of the microstructure as a function of ferrite grain size, martensite inclusion size, carbon content, and volume fraction of second phase not only for uniaxial tension but also for more complex biaxial loading involving change of loading paths.

### *3.3. TRIP assisted multiphase steels*

The microstructure of TRIP assisted multiphase steels is made of a ferrite/bainite matrix typically including 5 to 20% of retained austenite in the form of micron size inclusions. The retained austenite is metastable owing to a sufficiently large C content. Under mechanical loading, the mechanical work provides the extra driving force needed for the transformation of the austenite into martensite. In optimised TRIP steels, the stability of the austenite is designed such as to transform during a wide range of plastic deformation. The transformation has two direct effects on the mechanical response. First, it continuously introduces an increasing amount of a hard phase replacing the softer austenite. It is thus an evolving dual phase steel. Furthermore, the transformation is associated with dilatation and shear transformation strain components, involving additional strain hardening around the transformed inclusion. If the stability is properly tuned, these two effects then cooperate to produce an enhanced strength/ductility ratio, see e.g. [26,66,67]. All known modelling efforts, e.g. [26] neglect plastic strain gradients contributions to the TRIP effect, even though the size of the austenite inclusions is often close to 1 micrometre and sometimes smaller, or much smaller (example of interlath martensite). For instance, Delannay et al. [68], had to artificially increase the hardening in the ferrite to accurately capture the overall response of the material.

The model shown in Fig. 5a is made of a single retained austenite island surrounded by a ferrite matrix, itself included within a large region described with the mean response of the composite material. The goal of the surrounding homogenised medium is to allow imposing realistic boundary conditions to the single central unit cell, independent of the way the loading is controlled at the external surfaces, i.e. load or displacement controlled. The results of the model are analysed in terms of the response of the inner square cell made of ferrite and austenite inclusion. An ellipsoidal lens of austenite is transformed

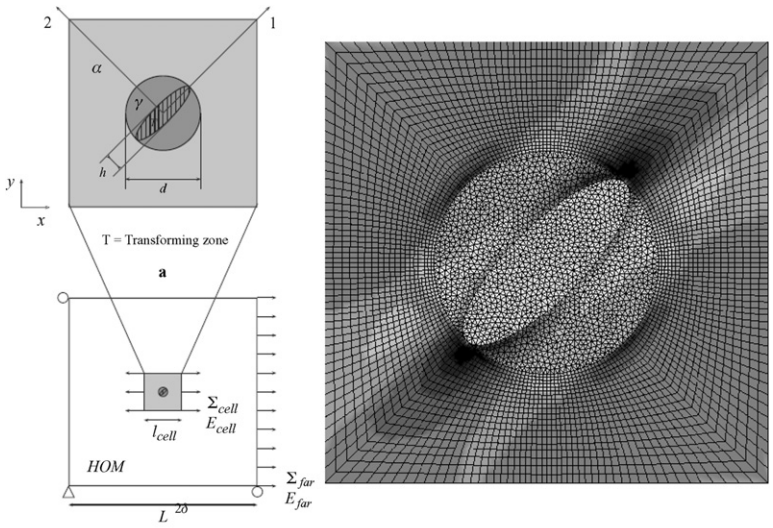


(a)

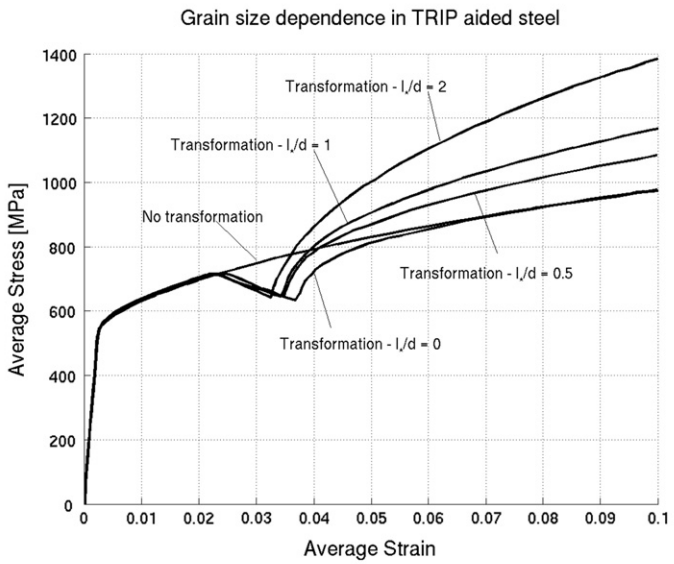


(b)

**Fig. 5.** Size effect on TRIP-aided steel: (a) embedded unit cell model and distribution of plastic strains induced by the martensitic transformation, (b) grain size dependence of the average response of the embedded cell as a result of the transformation.

into martensite according to an ad-hoc criterion, e.g. when a prescribed macroscopic strain level is attained, taken here equal to 2.25%. The interface between the austenite and the martensite was not present initially. It is thus introduced in the course of the calculation, and modelled as a hard boundary (zero plastic flow). The volume fraction of austenite is equal to 10% (inside the inner cell), with a size $d$. The plastic flow is characterised by a single length scale $l^*$, see [45] for more refined results with the three-length version of the model. The transforming zone represents 3% of the inner cell. The flow properties of the different phases are represented by a Swift law (8) and are given in Table 1.

Fig. 5b shows the evolution of the average tensile stress in the inner cell as a function of the average strain for calculations performed with the small strain version of the model. One curve, $l^*/d = 0$, corresponds to the response of the inner cell without any transformation and any size effect. The transformation is easily detected by a softening transient due to the dilatation of the transforming region. The first curve with transformation corresponds again to the response with a classical plasticity theory ($l^*/d = 0$). The effect of the transformation on the response, after the transient, is very small, providing almost the same strain hardening response as without transformation. Now, when the effect of the small size of the retained inclusion is taken into account, a very significant enhancement of the strain hardening capacity is observed, increasing with

**Table 1**
Properties of phases for the modelling of transformation effect in TRIP-aided steels (Swift hardening law).

| | Ferrite | Austenite | Martensite |
|---|---|---|---|
| $\sigma_0$ (MPa) | 475 | 700 | 2000 |
| $\varepsilon_0$ | 55 | 50 | 800 |
| $N$ | 0.27 | 0.3 | 0.05 |

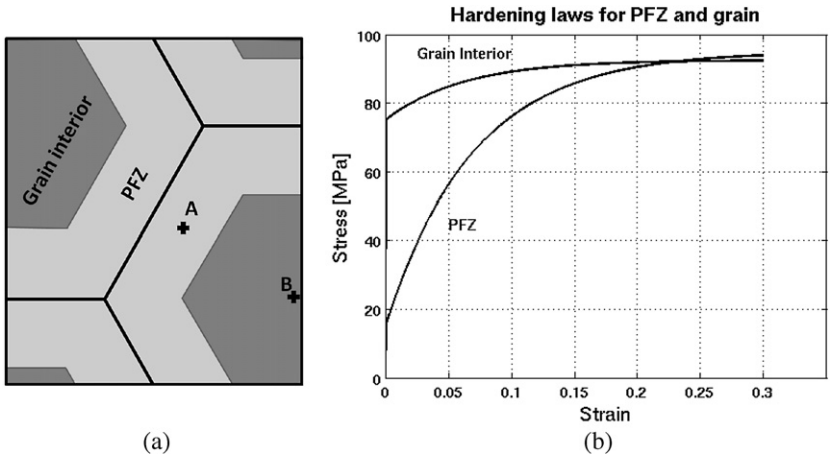


**Fig. 6.** Model parameters used for simulating Al alloys with precipitate free zones (PFZ); (a) unit cell used in the computations showing the location of the points used from which the field quantities presented in Figs. 8 and 9 are extracted (point A is located at the mid thickness of the PFZ, point B is located at the centre of the grain interior region), (b) Voce hardening laws used in the computations for both regions of the material.

decreasing $d$. Although there is no direct comparison possible with experiments, where the material involves a succession of transformation events at slightly different strains, the enhancement of the strain hardening is much more realistic in view of the high properties repetitively reported for TRIP steels. This shows that the austenite grain size is a key parameter on which one can play to optimise multiphase TRIP steels. Now, the size of the transformed zone is also known to affect the stability of the grain, and thus the evolution of the transformation. This is not taken into account in the current model which does not involve a true phase transformation criterion as such, see e.g. [69–71].

## 4. Size dependent response of precipitate free zones

A variety of Al, Ti, Ni or Fe based metallic alloys involve micron or submicron thick layers surrounding GB with a microstructure different from the bulk of the grain, e.g. [30–32]. Often, these layers are softer than the rest of the grain, due to the absence of hardening precipitates which populate the grain interior (see Fig. 1), hence the name precipitate free zones (PFZ). When the material is deformed, plasticity develops first inside the PFZ. The intense local plasticity gives rise to void nucleation on particles residing on the GB, causing, through a mechanism of growth and coalescence of voids, premature intergranular ductile failure. A classical example is given by the Al alloys of the 7xxx series with important implications in aeronautical applications [72,73]. The risk of intergranular failure increases with increasing strength mismatch between the PFZ and grain interior. If the mismatch is not too large, the strain hardening of the PFZ (which has a much larger strain hardening capacity than the grain interior) raises the strength up to a value corresponding to the strength of the grain interior before damage has accumulated to a critical point. Then, the initially hard grain becomes the softest region leading to a more classical ductile transgranular failure. This problem has received some attention in the literature with various efforts to predict the competition between failure modes based on ductile failure models. Nevertheless, all these efforts have neglected size dependent plasticity effects. Considering that the typical PFZ is thinner than 1 μm and sometimes thinner than 100 nm, the validity of this assumption is questionable. Here we investigate, using the model described in Section 2, the potential impact of the thickness of the PFZ on the evolution of the plastic flow and on the evolution of the strength mismatch.

The model shown in Fig. 6a is similar to the one used for the ferritic steel polycrystal except that a thin layer of material, with different properties is introduced along the GB. The thickness of the layer is noted $l_{PFZ}$. There are two types of interfaces in this case. The GB is modelled with the interface model described in Section 2.3. The interface between the soft and the hard zone is not a true physical interface. A dislocation is free to move from one zone to another, except that it undergoes a different resistance in the PFZ (intense forest hardening in the PFZ + accumulation of GNDs due to the GB barrier) and in the grain interior (precipitate hardening + forest hardening + some possible GNDs resulting from the GB barrier if the PFZ is very thin). Hence, the plastic flow is left unconstrained at this boundary.

**Table 2**
PFZ and grain interior hardening properties (Voce law) for the investigation of size effects on the transition between intergranular and transgranular failure modes in Al alloys with precipitate free zone (PFZ) along grain boundaries.

| | Grain interior | PFZ |
|---|---|---|
| $\sigma_0$ (MPa) | 75 | 15 |
| $\beta$ | 16.6 | 14.4 |
| $\theta_0$ (MPa) | 290 | 1150 |

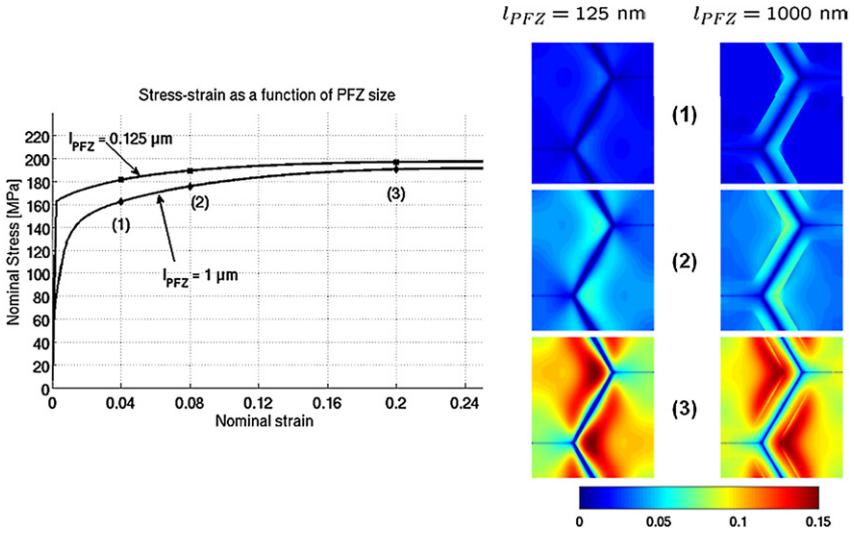


**Fig. 7.** Effect of the size of the precipitate free zone on the mechanical response: (left) tensile nominal response of the representative material cell, (right) distributions of the plastic strains in the unit cell for two extreme values of the PFZ.

The flow properties of each zone have been adapted from the one used in Ref. [72], in terms of a Voce law (7), see Table 2. The initial yield stress of the PFZ is fixed to 1/5 of the initial yield stress assumed for the interior of the grain. The corresponding hardening laws of both phases are depicted in Fig. 6b. A grain size of 10 µm (including the PFZ) is considered, with an intrinsic length $l_*$ equal to 0.5 µm for both the PFZ and the grain interior, in the range of values commonly adopted for the present strain gradient plasticity theory. The GBs are assumed permanently confining, and the size of the PFZ $l_{PFZ}$ is varied to investigate the potential size effects on the strain distribution and effect on the failure mode, with values ranging from 0.125 to 1 µm, corresponding to $l_{PFZ}/l_*$ ranging from 0.25 to 2.

The response of the representative material cell is depicted in Figs. 7 to 9. Fig. 7 shows the nominal stress–strain curves as well as the distribution of plastic strains inside the RVE for the thinnest (0.125 nm) and thickest (1 µm) PFZ. For a PFZ size on the order of 1 µm, the PFZ deforms much faster than the grain interior due to its lower strength. Considering the constraint due to the surrounding grain, the stress triaxiality will be large favouring an intergranular ductile failure mode [72]. Conversely, for a PFZ on the order of 125 nm, plastic deformation is virtually absent. This effect is the result of the strength enhancement associated with the steep gradients present in the PFZ at both the GB and (softer) interface with the grain interior. Another illustration of the effect of the PFZ size is provided in Figs. 8 and 9. The evolution of the plastic strain as a function of the macroscopic loading in typical positions inside the PFZ and at the centre of the grain is represented in Fig. 8. For thin PFZ, gradient effects on the hardening of the PFZ are such that the PFZ becomes almost immediately harder than the grain itself. As a consequence, the plastic strains in the grain are larger than in the PFZ over the entire loading range. Increasing the size of the PFZ decreases the gradient effects, hence decreasing its effective strength. As can be observed in Fig. 8, this results into larger plastic strains in the PFZ compared to the grain interior at the early stage of loading. The macroscopic strain at which the plastic deformation in the middle of the grain becomes larger than in the PFZ increases with the size of the PFZ. Fig. 9 provides the evolution of the von Mises stress at the different locations as a function of the PFZ size. Hence, the size of the PFZ definitely plays a role on the competition between intergranular and transgranular failure through a first order contribution to the hardening response of this initially soft layer. These results call for additional investigations coupled to a quantitative modelling of the damage mechanisms [72–74].

Note that in the present simulations, a global grain size (including the PFZ) of 10 µm is considered. This means that the grain interior zone has a variable size depending on the size of the PFZ. In the case of $l_{PFZ} = 1000$ nm, the grain interior is 8 µm wide, which may trigger some interaction gradient effects coming from the opposite GB. These are however considered negligible here since the ratio between the intrinsic length and the grain interior region is approximately 1/16, a ratio for which the gradient enhancement was found negligible for a comparable hardening law in [46].

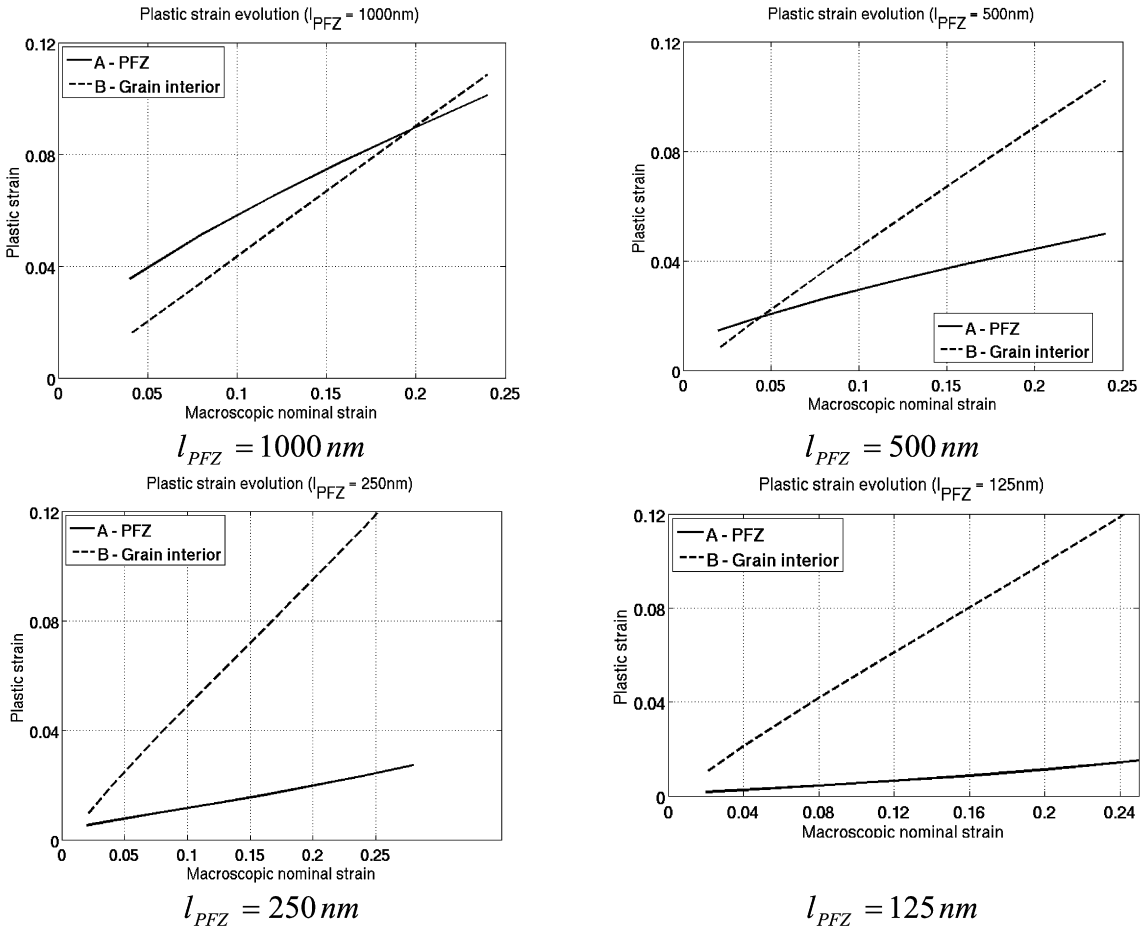


**Fig. 8.** Effect of the size of the precipitate free zone (PFZ) on plastic strain evolution in the PFZ compared to the grain interior.

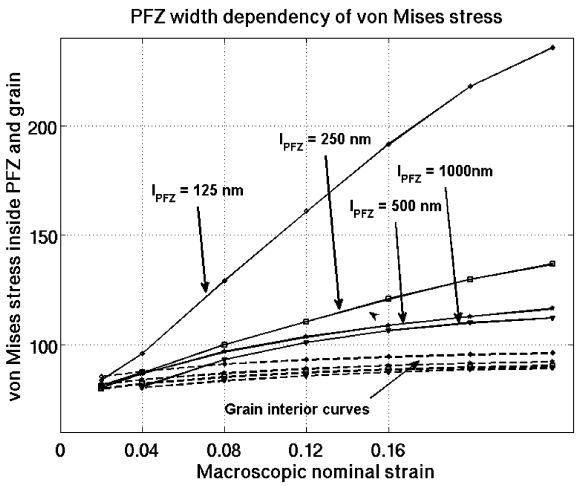


**Fig. 9.** Effect of the size of the precipitate free zone on the evolution of the equivalent von Mises stress in the PFZ and in the grain interior.

## 5. Conclusions

The generic interface model discussed in this paper, involving a thin layer described by a traction separation law and evolving higher order boundary conditions on both sides of the layer, is rich enough to empirically encompass a wide range of phenomena that constrain the plastic flow in a variety of metallic systems. The evolutionary character of the higher

order boundary conditions permits representing the creation of new barriers due, for instance, to phase transformation, the stress controlled transparency of an interface, for instance in the case of grain or twin boundaries, or the modification of the interface structure during loading, for instance a twin becoming less and less coherent with plastic flow [20]. For all the problems addressed in this work, the law dictating the evolution of the higher order boundary conditions and the parameters of the interface traction separation law have been identified using inverse modelling or simply imposed as realistic values. Future works should rely on atomistic models and/or dislocation dynamics to guide the form of the laws and to determine the values of the parameters. Obviously, this approach requires being connected to a higher order plasticity theory which will generate realistic gradient plasticity effects and associated back stress. Here, a rate independent isotropic model is used, but a crystal plasticity formulation with or without rate dependency will, for many problems, be more adapted. Even though the examples given here about ferritic and dual phase steels prove that the main effects related to the grain size can be captured with a single constant internal length, the issues related to the need for several internal lengths, possibly evolving, remain quite open, as for any empirical strain gradient plasticity approach.

## Acknowledgements

The support of the Belgian Science Policy through the IAP 6/24 project is gratefully acknowledged, as well as the support of FRS-FNRS through grant 1.5.032.09.F.

## References

[1] E. Arzt, G. Dehm, P. Gumbsch, O. Kraft, D. Weiss, Interface controlled plasticity in metals: dispersion hardening and thin film deformation, Prog. Mater. Sci. 46 (2001) 283–307.
[2] M.A. Meyers, A. Mishra, D.J. Benson, Mechanical properties of nanocrystalline materials, Prog. Mater. Sci. 51 (2006) 427–556.
[3] M. Dao, L. Lu, R.J. Asaro, J.T.M. De Hosson, E. Ma, Toward a quantitative understanding of mechanical behavior of nanocrystalline metals, Acta Mater. 55 (2007) 4041–4065.
[4] L. Zhu, H. Ruan, X. Li, M. Dao, H. Gao, J. Lu, Modeling grain size dependent optimal twin spacing for achieving ultimate high strength and related high ductility in nanotwinned metals, Acta Mater. 59 (2011) 5544–5557.
[5] N.A. Fleck, J.W. Hutchinson, Strain gradient plasticity, Adv. Appl. Mech. 33 (1997) 295–361.
[6] A. Needleman, J. Gil Sevillano, Preface to the viewpoint set on: geometrically necessary dislocations and size dependent plasticity, Scripta Mater. 48 (2003) 109–111.
[7] P. Gudmundson, A unified treatment of strain gradient plasticity, J. Mech. Phys. Solids 52 (2004) 1379–1406.
[8] M.G.D. Geers, W.A.M. Brekelmans, C.J. Bayley, Second-order crystal plasticity: internal stress effects and cyclic loading, Modell. Simul. Mater. Sci. Eng. 15 (2007) 133–145.
[9] N.A. Fleck, J.R. Willis, A mathematical basis for strain-gradient plasticity theory. Part II: Tensorial plastic multiplier, J. Mech. Phys. Solids 57 (2009) 1045–1057.
[10] M.E. Gurtin, L. Anand, Nanocrystalline grain boundaries that slip and separate: A gradient theory that accounts for grain-boundary stress and conditions at a triple-junction, J. Mech. Phys. Solids 56 (2008) 184–199.
[11] R.K. Abu Al-Rub, G.Z. Voyiadjis, A physically based gradient plasticity theory, Int. J. Plasticity 22 (2006) 654–684.
[12] W.A.T. Clark, R.H. Wagoner, Z.Y. Shen, T.C. Lee, I.M. Robertson, H.K. Birnbaum, On the criteria for slip transmission across interfaces in polycrystals, Scripta Metall. Mater. 26 (1992) 203–206.
[13] H. Van Swygenhoven, P.M. Derlet, A.G. Froseth, Nucleation and propagation of dislocations in nanocrystalline fcc metals, Acta Mater. 54 (2006) 1975–1983.
[14] A. Ma, F. Roters, D. Raabe, On the consideration of interactions between dislocations and grain boundaries in crystal plasticity finite element modeling – Theory, experiments, and simulations, Acta Mater. 54 (2006) 2181–2194.
[15] T. Gorkaya, K.D. Molodov, D.A. Molodov, G. Gottstein, Concurrent grain boundary motion and grain rotation under an applied stress, Acta Mater. 59 (2011) 5674–5680.
[16] F. Mompiou, M. Legros, D. Caillard, SMIG model: A new geometrical model to quantify grain boundary-based plasticity, Acta Mater. 58 (2010) 3676–3689.
[17] J.W. Christian, S. Mahajan, Deformation twinning, Prog. Mater. Sci. 39 (1995) 1–157.
[18] K. Lu, L. Lu, S. Suresh, Strengthening materials by engineering coherent internal boundaries at the nanoscale, Science 324 (2009) 349–352.
[19] Z.X. Wu, Y.W. Zhang, D.J. Srolovitz, Dislocation–twin interaction mechanisms for ultrahigh strength and ductility in nanotwinned metals, Acta Mater. 57 (2009) 4508–4518.
[20] H. Idrissi, M.S. Colla, B. Wang, D. Schrijvers, J.P. Raskin, T. Pardoen, Strength and ductility of nanocrystalline freestanding palladium films, Adv. Mater. 23 (18) (2011) 2119–2122.
[21] O. Bouaziz, S. Allain, C. Scott, Effect of grain and twin boundaries on the hardening mechanisms of twinning-induced plasticity steels, Scripta Mater. 58 (2008) 484–487.
[22] J. Gil Sevillano, An alternative model for the strain hardening of FCC alloys that twin, validated for twinning-induced plasticity steel, Scripta Mater. 60 (2009) 336–339.
[23] H. Idrissi, K. Renard, L. Ryelandt, D. Schryvers, P.J. Jacques, On the mechanism of twin formation in Fe–Mn–C TWIP steels, Acta Mater. 58 (2010) 2464–2476.
[24] R.G. Stringfellow, D.M. Parks, G.B. Olson, A constitutive model for transformation plasticity accompanying strain-induced martensitic transformations in metastable austenitic steels, Acta Metall. Mater. 40 (1992) 1703–1716.
[25] F.D. Fischer, G. Reisner, E. Werner, K. Tanaka, G. Cailletaud, T. Antretter, A new view on transformation induced plasticity (TRIP), Int. J. Plasticity 16 (2000) 723–748.
[26] F. Lani, Q. Furnémont, T. Van Rompaey, F. Delannay, P.J. Jacques, T. Pardoen, Multiscale mechanics of TRIP-assisted multiphase steels: II. Micromechanical modelling, Acta Mater. 55 (2007) 3695–3705.
[27] P.J. Jacques, Q. Furnemont, S. Godet, T. Pardoen, K.T. Conlon, F. Delannay, Micromechanical characterisation of TRIP-assisted multiphase steels by in situ neutron diffraction, Phil. Mag. 86 (2006) 2371–2392.
[28] V. Gerold, Precipitation hardening, in: Dislocations in Solids, North-Holland Publishing Company, Amsterdam, 1979.

[29] A. Simar, Y. Bréchet, B. de Meester, A. Denquin, T. Pardoen, Modeling microstructures and local tensile properties of friction stir welds in aluminum alloy 6005A-T6, Acta Mater. 55 (2007) 6133–6143.
[30] D. Dumont, A. Deschamps, Y. Bréchet, A model for predicting fracture mode and toughness in 7000 series aluminium alloys, Acta Mater. 52 (2004) 2529–2540.
[31] T.F. Morgeneyer, M.J. Starink, S.C. Wang, I. Sinclair, Quench sensitivity of toughness in an Al alloy: Direct observation and analysis of failure initiation at the precipitate-free zone, Acta Mater. 56 (2008) 2872–2884.
[32] T. Krol, D. Baither, E. Nembach, The formation of precipitate free zones along grain boundaries in a superalloy and the ensuing effects on its plastic deformation, Acta Mater. 52 (2004) 2095–2108.
[33] J.P. Hirth, J. Lothe, Theory of Dislocations, Wiley, 1982 (1st edition, McGraw–Hill, 1968).
[34] L.B. Freund, S. Suresh, Thin Film Materials, 1st edition, Cambridge University Press, ISBN 0521822815, 2003.
[35] S. Puri, A. Das, A. Acharya, Mechanical response of multicrystalline thin films in mesoscale field dislocation mechanics, J. Mech. Phys. Solids 59 (11) (2011) 2400–2417.
[36] C. Brugger, M. Coulombier, T.J. Massart, J.-P. Raskin, T. Pardoen, Strain gradient plasticity analysis of the strength and ductility of thin metallic films using enriched interface model, Acta Mater. 58 (2010) 4940–4949.
[37] N.A. Fleck, G.M. Muller, M.F. Ashby, J.W. Hutchinson, Strain gradient plasticity: theory and experiment, Acta Metall. Mater. 42 (1994) 475–487.
[38] J.S. Stölken, A.G. Evans, A microbend test method for measuring the plasticity length scale, Acta Mater. 46 (1998) 5109–5115.
[39] M.E. Gurtin, A theory of grain boundaries that accounts automatically for grain misorientation and grain-boundary orientation, J. Mech. Phys. Solids 56 (2008) 640–662.
[40] K.E. Aifantis, J.R. Willis, Scale effects induced by strain-gradient plasticity and interfacial resistance in periodic and randomly heterogeneous media, Mech. Mater. 38 (2006) 702–716.
[41] N.A. Fleck, J.R. Willis, A mathematical basis for strain-gradient plasticity theory – Part I: Scalar plastic multiplier, J. Mech. Phys. Solids 57 (2009) 161–177.
[42] U. Borg, C.F. Niordson, J.W. Kysar, Size effects on void growth in single crystals with distributed voids, Int. J. Plasticity 24 (2008) 688–701.
[43] M.I. Hussein, U. Borg, C.F. Niordson, V.S. Deshpande, Plasticity size effects in voided crystals, J. Mech. Phys. Solids 56 (2008) 114–131.
[44] L. Mazzoni-Leduc, T. Pardoen, T.J. Massart, Strain gradient plasticity analysis of transformation induced plasticity in multiphase steels, Int. J. Solids Struct. 45 (2008) 5397–5418.
[45] L. Mazzoni-Leduc, T. Pardoen, T.J. Massart, Strain gradient plasticity analysis of the size effects associated to the transformation strain in TRIP steels, Eur. J. Mech. A – Solids 29 (2010) 132–142.
[46] T.J. Massart, T. Pardoen, Strain gradient plasticity analysis of the size dependent strength and ductility in single phase metals with evolving grain boundary confinement, Acta Mater. 58 (2010) 5768–5781.
[47] T.J. Massart, T. Pardoen, Strain gradient plasticity analysis of hardening in dual phase steels with enhanced higher order interface conditions, submitted for publication.
[48] N.A. Fleck, J.W. Hutchinson, A reformulation of strain gradient plasticity, J. Mech. Phys. Solids 49 (2001) 2245–2271.
[49] C.F. Niordson, P. Redanz, Size-effects in plane strain sheet-necking, J. Mech. Phys. Solids 52 (2004) 2431–2454.
[50] C.F. Niordson, V. Tvergaard, Instabilities in power law gradient hardening materials, Int. J. Solids Struct. 42 (2005) 2559–2573.
[51] A.G. Evans, J.W. Hutchinson, A critical assessment of theories of strain gradient plasticity, Acta Mater. 57 (2009) 1675–1688.
[52] R.M. McMeeking, J.R. Rice, Finite-element formulations for problems of large elastic–plastic deformation, Int. J. Solids Struct. 11 (1975) 601–616.
[53] E.O. Hall, The deformation and ageing of mild steel: III. Discussion of results, Proc. Phys. Soc. B 64 (1951) 747–753.
[54] A.S. Argon, Strengthening Mechanisms in Crystal Plasticity, Oxford Series on Materials Modelling, Oxford University Press, 2008.
[55] O. Bouaziz, T. Iung, M. Kandel, C. Lecomte, Physical modelling of microstructure and mechanical properties of dual-phase steel, J. Phys. IV France 11 (PR4) (2001) 223–231.
[56] S. Takaki, K. Kawasaki, Y. Kimura, Mechanical properties of ultra fine grained steels, J. Mater. Proc. Tech. 117 (2001) 359–363.
[57] D. Jia, K.T. Ramesh, E. Ma, Effects of nanocrystalline and ultrafine grain sizes on constitutive behavior and shear bands in iron, Acta Mater. 51 (2003) 3495–3509.
[58] N. Tsuji, Y. Ito, Y. Saito, Y. Minamino, Strength and ductility of ultrafine grained aluminum and iron produced by ARB and annealing, Scripta Mater. 47 (2002) 893–899.
[59] O. Bouaziz, A. Aouafi, S. Allain, Effect of grain refinement on the mechanical behaviour of ferritic steels: Evolution of isotropic hardening and kinematic hardening, Mater. Sci. Forum 584–586 (2008) 605–609.
[60] C.Y. Yu, P.W. Kao, C.P. Chang, Transition of tensile deformation behaviors in ultrafine-grained aluminum, Acta Mater. 53 (2005) 4019–4028.
[61] G.R. Speich, in: Fundamentals of Dual-Phase Steels, AIME, Warrendale, PA, 1981.
[62] M. Delincé, P.J. Jacques, Y. Bréchet, J.D. Embury, M.G.D. Geers, T. Pardoen, Microstructure based strain hardening model for the uniaxial flow properties of ultrafine grained dual phase steels, Acta Mater. 55 (2007) 2337–2350.
[63] M. Delincé, P.J. Jacques, T. Pardoen, Separation of size-dependent strengthening contributions in fine grained dual phase steels by nanoindentation, Acta Mater. 54 (2006) 3395–3404.
[64] G. Krauss, Deformation and fracture in martensitic carbon steels tempered at low temperatures, Metall. Mater. Trans. B 32 (2001) 205–221.
[65] S. Cobo, O. Bouaziz, Investigations and modelling of the work hardening of as quenched martensite, in: Proceedings of New Developments on Metallurgy and Applications of High Strength Steels, Buenos Aires, 2008, pp. 909–918.
[66] P. Jacques, Q. Furnémont, T. Pardoen, F. Delannay, On the role of martensitic transformation on damage and cracking resistance in TRIP-assisted multiphase steels, Acta Mater. 49 (1) (2001) 139–152.
[67] C. Herrera, D. Ponge, D. Raabe, Design of a novel Mn-based 1 GPa duplex stainless TRIP steel with 60% ductility by a reduction of austenite stability, Acta Mater. 59 (2011) 4653–4664.
[68] L. Delannay, P.J. Jacques, T. Pardoen, Prediction of the plastic flow of TRIP-aided multiphase steel based on an incremental mean-field model, Int. J. Solids Struct. 45 (2008) 1825–1843.
[69] F.D. Fischer, G. Reisner, A criterion for the martensitic transformation of a microregion in an elastic plastic material, Acta Mater. 46 (1998) 2095–2102.
[70] V.I. Levitas, Thermomechanical theory of martensitic phase transformations in inelastic materials, Int. J. Solids Struct. 35 (1998) 889–940.
[71] T. Van Rompaey, F. Lani, P. Jacques, B. Blanpain, P. Wollants, T. Pardoen, 3D embedded cell model for the martensitic transformation in TRIP-assisted multiphase steels, Metal. Mater. Trans. A 37 (2006) 99–107.
[72] T. Pardoen, D. Dumont, A. Deschamps, Y. Bréchet, Grain boundary versus transgranular ductile failure, J. Mech. Phys. Solids 51 (2003) 637–665.
[73] T. Pardoen, F. Scheyvaerts, A. Simar, C. Tekoğlu, P.R. Onck, Multiscale modeling of ductile failure in metallic alloys, C. R. Physique 11 (2010) 326–345.
[74] D. Steglich, W. Brocks, J. Heerens, T. Pardoen, Anisotropic ductile damage modelling of Al2024 alloys, Eng. Fract. Mech. 75 (2008) 3692–3706.